Revisiting the spectral and timing properties of 4U 1909+07 with *NuSTAR* and *Astrosat*

Gaurava K. Jaisawal[1]⋆, Sachindra Naik[2], Wynn C.G. Ho[3], Neeraj Kumari[2,4],
Prahlad Epili[5], and Georgios Vasilopoulos[6]

[1] *National Space Institute, Technical University of Denmark, Elektrovej 327-328, DK-2800 Lyngby, Denmark*
[2] *Astronomy and Astrophysics Division, Physical Research Laboratory, Navrangapura, Ahmedabad - 380009, Gujarat, India*
[3] *Department of Physics and Astronomy, Haverford College, 370 Lancaster Avenue, Haverford, PA, 19041, USA*
[4] *Indian Institute of Technology, Gandhinagar - 382355, Gujarat, India*
[5] *School of Physics and Technology, Wuhan University, Wuhan 430072, China*
[6] *Department of Astronomy, Yale University, PO Box 208101, New Haven, CT 06520-8101, USA*

26 August 2020

ABSTRACT

We present the results obtained from the analysis of high mass X-ray binary pulsar 4U 1909+07 using *NuSTAR* and *Astrosat* observations in 2015 and 2017 July, respectively. X-ray pulsations at ≈604 s are clearly detected in our study. Based on the long term spin-frequency evolution, the source is found to spun up in the last 17 years. We observed a strongly energy-dependent pulse profile that evolved from a complex broad structure in soft X-rays into a profile with a narrow emission peak followed by a plateau in energy ranges above 20 keV. This behaviour ensured a positive correlation between the energy and pulse fraction. The pulse profile morphology and its energy-evolution are almost similar during both the observations, suggesting a persistent emission geometry of the pulsar over time. The broadband energy spectrum of the pulsar is approximated by an absorbed high energy exponential cutoff power law model with iron emission lines. In contrast to the previous report, we found no statistical evidence for the presence of cyclotron absorption features in the X-ray spectra. We performed phase-resolved spectroscopy by using data from the *NuSTAR* observation. Our results showed a clear signature of absorbing material at certain pulse-phases of the pulsar. These findings are discussed in terms of stellar wind distribution and its effect on the beam geometry of this wind-fed accreting neutron star. We also reviewed the subsonic quasi-spherical accretion theory and its implication on the magnetic field of 4U 1909+07 depending on the global spin-up rate.

Key words:
stars: neutron – pulsars: individual: 4U 1909+07 – X-rays: stars.

1 INTRODUCTION

High mass X-ray binaries (HMXBs) are known to consist of a compact object (mostly a neutron star) and a massive (>10 $M_\odot$) OB optical companion in a close binary (see, e.g., Lewin et al. 1997; Tauris & van den Heuvel 2006). The material from the companion primarily gets accreted onto the neutron star by falling into its deep gravitation potential. This process releases an enormous amount of energy, mostly in the X-ray range of the electromagnetic spectrum. Depending on the nature of the optical companion, the mass transfer can take place differently between two sub-classes of HMXBs viz. super-giant X-ray binaries and Be/X-ray binaries. The compact object in super-giant X-ray binaries (SGXBs) captures sporadically

a small fraction of the stellar wind from its super-giant companion which loses mass at a rate of $10^{-5} - 10^{-7}$ $M_\odot$ yr^{-1} (Martínez-Núñez et al. 2017). The luminosity of the compact object reaches as high as 10^{35} erg s^{-1} in most of SGXBs. Luminosity with one to three orders of magnitude higher has also been observed from a couple of SGXB systems such as Cen X-3, SMC X-1, and LMC X-4 where a disk-fed accretion via the Roche-lobe overflow occurs (see, e.g., Reig 2011; Walter et al. 2015).

Be/X-ray binary (BeXB) systems represent a majority of the HMXB population. It consists of a neutron star and a non-supergiant donor of OB spectral class that shows hydrogen and helium emission lines at a certain point of its evolution (Reig 2011 for a review). These emission lines are known to originate from an equatorial circumstellar disk formed around the Be star (Porter & Rivinius 2003). The neutron star in these systems usually revolves

⋆ E-mail: gaurava@space.dtu.dk

in a wide, eccentric orbit and is known to accrete matter from the circumstellar disk. The abrupt mass accretion by the neutron star, at the closest approach (periastron), leads to the occurrence of intense X-ray outbursts with luminosity in the range of 10^{36}–10^{38} erg s^{-1} (Naik et al. 2013; Reig & Nespoli 2013; Wilson-Hodge et al. 2018; Jaisawal et al. 2019).

Strong magnetic field of the neutron stars, with a field strength of B~10^{12} G in HMXBs, guides the accreted matter beyond the magnetospheric radius (Revnivtsev & Mereghetti 2015). The field lines funnel the plasma onto a confined region at the magnetic poles forming hot spots and accretion columns on the neutron star surface (Basko & Sunyaev 1975; Nagase 1989). X-ray pulsations from the neutron star are observed when the hot spot rotates around the spin axis of the system. Pulse profiles of these pulsating neutron stars (pulsars) provide information on emission geometry and also on the distribution of matter in its close proximity. A typical energy spectrum of a pulsar is shaped by thermal and bulk Comptonization processes in the accretion column (Becker & Wolff 2007; Farinelli et al. 2012) that can be described by an empirical power law model modified with a high energy cutoff (see, e.g., White et al. 1983; Paul & Naik 2011; Caballero & Wilms 2012).

4U 1909+07 (X 1908+075) is a Galactic X-ray source that was discovered by *Uhuru* in the early seventies (Giacconi et al. 1974; Forman et al. 1978; Wen et al. 2000). The compact object in this system accretes from an OB supergiant companion in a 4.4 days orbit (Wen et al. 2000; Levine et al. 2004; Morel & Grosdidier 2005). 605 s pulsations detected from the *RXTE* observations, established the source as an accreting X-ray pulsar (Levine et al. 2004). Using the Doppler delay curves, the orbital parameters of the system such as the inclination (38°–72°), orbital separation (60–80 lt-s), epoch for mean longitude of 90 degrees τ_{90} (52631.383 MJD) along with the mass of the companion (9–31 $M_\odot$) and radius (≤ 22 $R_\odot$) were derived by Levine et al. (2004). The optical companion was first thought to be a Wolf-Rayet star based on the X-ray analysis (Levine et al. 2004). Near-infrared observations of the field within the error box of HEAO-1/A3 discovered a late O-type supergiant star (Morel & Grosdidier 2005). Recently, Martínez-Núñez et al. (2015) studied the H- and K-band infrared spectra of the optical companion using a non-LTE stellar atmosphere code and found the donor properties are mainly consistent with an early B-type (B0–B3) star. These authors also estimated the following donor parameters such as the stellar mass 15±6 $M_\odot$, radius 16 $R_\odot$, the effective temperature T$_*$ = 23.0$^{+6}_{-3}$ × 10^3 K, luminosity log(L/$L_\odot$) = 4.81±0.25, and the terminal wind velocity v_∞ = 500±100 km s^{-1}. The source distance is known to be 4.85±0.5 kpc depending on the extinction curve (Martínez-Núñez et al. 2015).

Long term timing studies showed that the spin period of the pulsar changes erratically on years time scale. It is only possible when mass accretion through the capture of stellar wind occurs in the system (Fürst et al. 2011, 2012). A similar conclusion was drawn based on the detection of the Compton shoulder in the iron fluorescence line. Such a line feature appears when the Compton thick medium surrounds the accreting object (Torrejón et al. 2010). The pulse profile of the pulsar is known to be strongly energy dependent. It evolves from a broad structure in soft X-rays to a narrow peak at higher energies (Fürst et al. 2011, 2012; Jaisawal et al. 2013). Broad-band energy spectrum of the pulsar is consistent with an absorbed high energy cutoff power law model along with a blackbody component (Fürst et al. 2011, 2012; Jaisawal et al. 2013). Based on a possible/tentative detection of cyclotron absorption line at ~44 keV (Jaisawal et al. 2013), the magnetic field of the neutron star is estimated to be ~3.8×10^{12} G. Superorbital modula-

Table 1. Log of 4U 1909+07 observations with *NuSTAR*, *Swift*, and *Astrosat*.

Observatory/ Instrument	ObsID	Start Date (MJD)	Expo. (ks)
NuSTAR	30101050002	57204.65	41.3
Swift/XRT	00081661001	57205.38	1.7
Astrosat	A03_114T01_9000001390	57951.27	30.3

tion at a period of 15.2 days is also known from the system (Corbet & Krimm 2013).

In the present paper, we study the pulse profile and spectral evolution of 4U 1909+07 using *NuSTAR* and *Astrosat* observations in 2015 and 2017 July, respectively. We examine the distribution of stellar wind during these monitorings. The spin period evolution of the pulsar is also studied based on the long term measurements. The details of the observations, results, discussion, and conclusion are summarized in Section 2, 3, and 4, respectively.

2   OBSERVATIONS AND DATA ANALYSIS

2.1   *NuSTAR* and *Swift*

NuSTAR is a first hard X-ray focusing observatory that was launched by NASA in 2012 June (Harrison et al. 2013). It is sensitive in 3–79 keV energy range and reflects the photons at grazing angle incidence. *NuSTAR* consists of two multi-layer coated focal plane mirror modules, named as FPMA and FPMB. 4U 1909+07 was observed with *NuSTAR* on 2015 July 01 for exposure of 41.3 ks (Table 1). Standard procedures were followed to analyze the raw data with the help of `NuSTARDAS` 1.6.0 software in HEASoft version 6.24. We reprocessed unfiltered events from the FPMA and FPMB by using *nupipeline* routine and updated CALDB of version 20191219. We then extracted source products by selecting a circular region of 150 arcsec radius with the source co-ordinates as the center, in the DS9 image of cleaned events, using the *nuproducts* task. The background light curves and spectra were accumulated in a similar manner by selecting a source-free circular region of 150 arcsec radius. 4U 1909+07 was also monitored by *Swift*/XRT on 2015 July 02 for an effective exposure of 1.7 ks in photon counting mode. We considered *Swift* observation for contemporary spectral analysis with *NuSTAR*. The XRT data are processed by using the online standard tools provided by the UK Swift Science Data Centre[1] (Evans et al. 2009). For timing analysis, the light curves from FPMA and FPMB units of *NuSTAR* were combined in our study.

2.2   *Astrosat*

Astrosat is the first Indian astronomical mission launched by ISRO in September 2015 (Agrawal 2006). It is capable of observing stellar sources in multi-wavelength bands by using five sets of instruments such as Soft X-ray Telescope (SXT; Singh et al. 2017), Large Area X-ray Proportional Counters (LAXPCs; Agrawal et al. 2017; Antia et al. 2017), Cadmium Zinc Telluride Imager (CZTI; Rao et al. 2017), a Scanning Sky Monitor (SSM; Ramadevi et al. 2018),

---

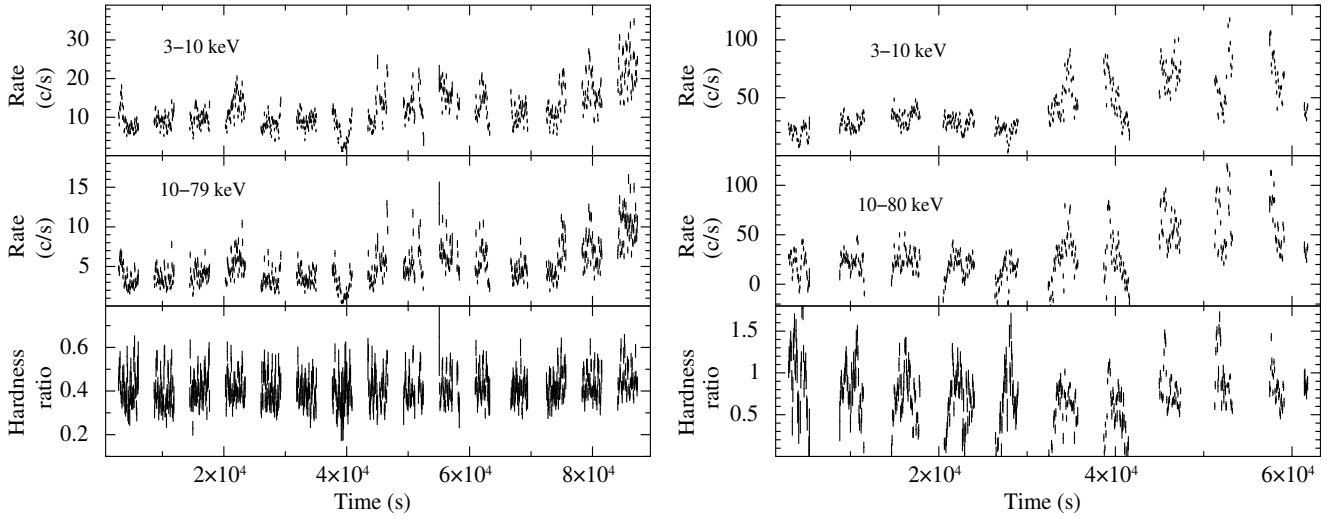[1] http://www.swift.ac.uk/user_objects/

Figure 1. Soft and hard X-ray light curves of the pulsar 4U 1909+07 obtained from the *NuSTAR* (left) and *Astrosat*/LAXPC (right) observations at one tenth time resolution of the spin period are shown in top two panels of the figure. Several flare-like features are visible in the light curve. A ratio between the hard and soft X-ray light curves i.e. hardness ratio is also presented in respective bottom panels.
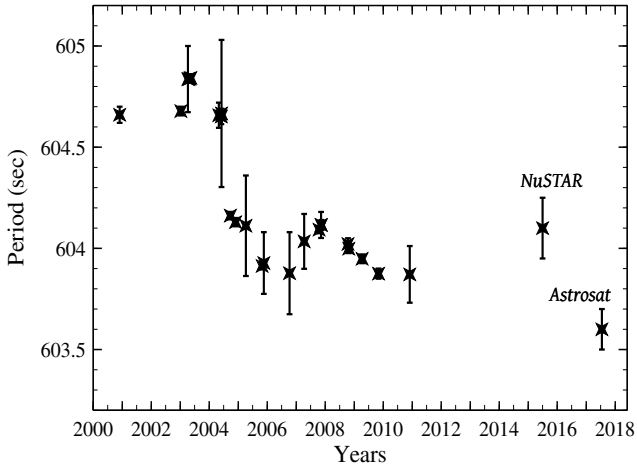

Figure 2. Long term spin period evolution of 4U 1909+07 based on measurements provided by Levine et al. (2004), Fürst et al. (2011), Fürst et al. (2012), and Jaisawal et al. (2013) using *RXTE*, *INTEGRAL*, and *Suzaku* data. The spin period measurements from the recent *NuSTAR* and *Astrosat* observations are also included in the figure.

.

and Ultraviolet Imaging Telescope (UVIT; Tandon et al. 2017). *Astrosat* observed 4U 1909+07 on 2017 July 17 for an effective exposure of 30.3 ks. In the present study, we used data from the SXT and LAXPC instruments as the source was very faint for the CZTI. The UVIT was not operational during the observation. The SXT is a soft X-ray focusing telescope consisting of a CCD detector sensitive in a 0.3-8 keV energy range. We reprocessed the SXT data by using standard pipeline and merging tool `sxtevtmergertool` provided by *Astrosat* Science Support Cell (ASSC[2]). The source spectrum was extracted thereafter using `XSELECT` package by considering a
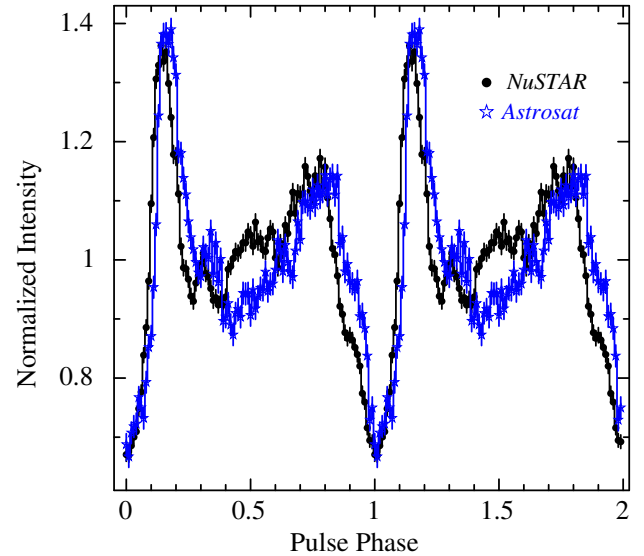
Figure 3. Pulse profiles of 4U 1909+07 obtained from the 2015 July and 2017 July observations with *NuSTAR* and *Astrosat* in a 3-79 keV range, respectively. The structure of the pulse profiles from both the instruments in broad energy range is found to be almost identical except a major difference at around 0.5 phase. Pulse profiles are normalized with respect to average intensity. The error bars represent 1σ uncertainties. Two pulses are shown for clarity. The pulse profiles from *NuSTAR* and *Astrosat* data are obtained by considering 100 phase bins per period.

circular region of 4 arcmin radius with source coordinates as centre, on the SXT CCD chip. The background spectrum was obtained from a blank sky observation. The LAXPC is the primary X-ray instrument onboard *Astrosat* which is sensitive to photons in a 3-80 keV energy range. It consists of three identical units providing a total effective area of 6000 cm^2 at 15 keV. In our study, the raw event analysis mode data are reprocessed through the standard routines available in `LAXPCsoftware`. We used this package to create source light curves and spectral products. The same observation was considered for the LAXPC background during the Earth occul-
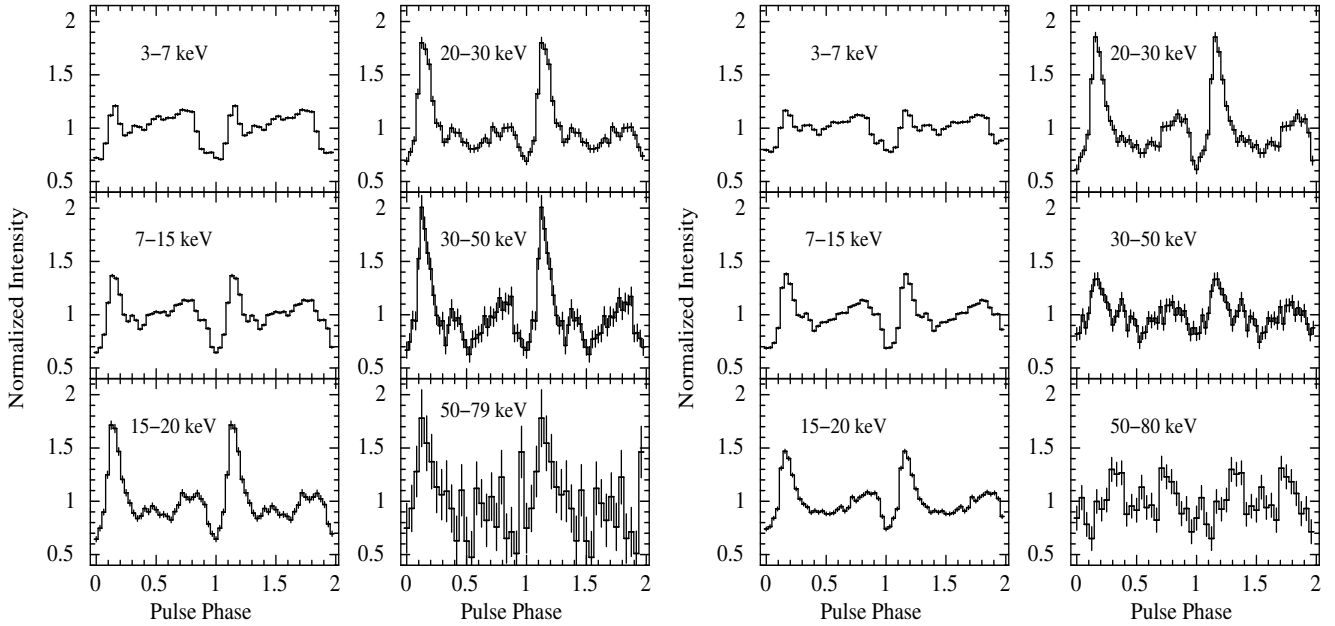
Figure 4. Energy resolved pulse profiles of 4U 1909+07 obtained by folding the light curves from *NuSTAR* (left) and *Astrosat*/LAXPC (right) observations with the estimated spin periods. Two pulses are shown in each panel for clarity. The error-bars represent 1σ uncertainties.
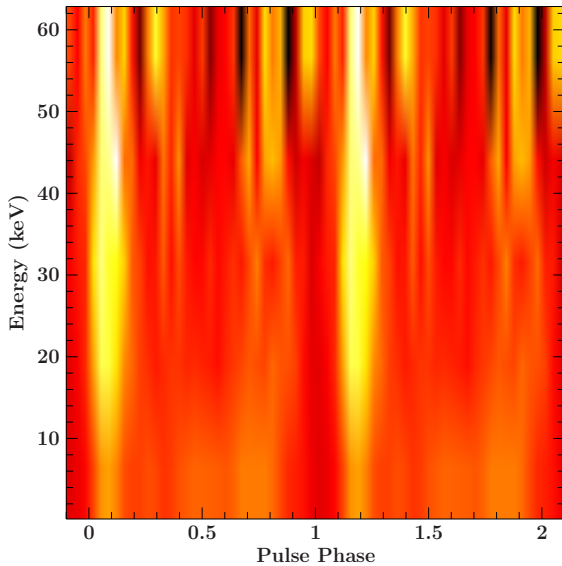

Figure 5. Color-coded pulse profile map produced from the energy resolved light curves of the pulsar using *NuSTAR* data in 2015 July. The color in the figure represents the normalized intensity of the profile, varying from red (low) to white (high). Two pulses are shown for clarity.

tation period. For timing studies, we have combined the light curves from LAXPC10 & 20 in our analysis. The data from LAXPC30 are not used due to drastic change in the instrument gain.

3   RESULTS

3.1   Timing analysis

Using the orbital ephemeris of the binary system as reported by Levine et al. (2004), we found that the pulsar was observed in 0.215–0.437 and 0.87–0.05 phase ranges of the 4.4 days binary orbit with *NuSTAR* and *Astrosat* observatories, respectively. Background subtracted light curves obtained from these observations are shown in Figure 1. Flare-like features can be seen in the soft and hard X-ray light curves (top two panels in each side of the figure) as generally seen in the light curves of other SGXBs due to inhomogeneous mass accretion from the stellar wind of the companion star (see, e.g., Naik et al. 2011; Odaka et al. 2013). Bottom panel in each side of the figure represents the hardness ratio (HR) which is defined as the ratio between the hard X-ray (10-79 keV range for *NuSTAR* data and 10-80 keV range for *Astrosat*/LAXPC data) and soft X-ray (3-10 keV range) light curves. Though we observe several flare-like features in the soft and hard X-ray light curves, the HRs remain almost constant throughout these monitoring. This suggests that the spectral shape of the pulsar was unchanged during the *NuSTAR* and *Astrosat* observations.

We searched for pulsation in the X-ray light curves by using the χ^2-maximization technique (Leahy 1987). The barycentric corrected pulse period of the neutron star was estimated to be 604.1±0.15 s and 603.6±0.1 s from the *NuSTAR* and *Astrosat* light curves binned at a time resolution of 0.1 s, respectively. The errors in the pulse period are estimated for a 1σ confidence interval.

Pulsation periods and the associated uncertainties were also calculated by fitting the pulse times of arrival (TOA) with a timing model. We followed the methodology described by Ray et al. (2011), that has been applied to other HMXB pulsars (Ray et al. 2019b; Vasilopoulos et al. 2019, 2020). We subdivided the data into 10-20 intervals and generated TOAs by comparing the pulse profile of each interval with a template profile. We fitted the TOAs to a timing model with constant period. The best pulse period is consistent

with the main peak found with the epoch folding method, while uncertainties were found to be of the order of 0.06-0.1 s. Nevertheless, the solution has some timing residuals likely caused by changes of the pulse profile within each observation.

Long term spin period evolution of 4U 1909+07 is given in Figure 2. The spin periods of the pulsar at earlier epochs were taken from Levine et al. (2004), Fürst et al. (2011), Fürst et al. (2012), and Jaisawal et al. (2013) using *RXTE*, *INTEGRAL*, and *Suzaku* data. We also included our pulse period measurements in the figure that clearly signifies a global spin-up trend of the pulsar since its discovery, though a sharp drop in the period has been observed during 2004–2005. The pulse period is effectively changed from 604.7 s to 603.6 s between 2001–2017 resulting an average spin-up rate $\dot{P}$ of 1.71×10^{-9} s s^{-1}.

Following the estimation of spin period of 4U 1909+07, the light curves from *NuSTAR* (FPMA+FPMB) and added light curves of LAXPC10 and LAXPC20 of *Astrosat* are folded with respective periods to obtain corresponding pulse profiles. The pulse profiles of the pulsar with 100 phase bins per period, obtained from both the data sets are shown in Figure 3. The observed pulse morphology shows a narrow emission peak at around 0.1 phase, followed by a broad structure at other pulse phases. The emission geometry appears to be similar during the 2015 and 2017 observations, though marginal differences can be spotted at certain pulse phases, especially at ∼0.5 phase, see Figure 3. To understand the energy evolution of the emission geometry, the energy resolved pulse profiles are generated and shown in Figure 4. Using *NuSTAR* data, we observed a broad profile below 7 keV that evolves into a narrow emission peak, followed by a plateau like structure at higher energies (left side of Figure 4). The color-coded pulse profile map shows this variation clearly (Figure 5). This map is generated by using `ISISscripts`[3]. The color in the map represents the normalized intensity of the pulse profiles ranging from red (low) to white (high). A similar kind of pulse profile evolution is also detected during the *Astrosat* observation with a clear difference above 30 keV (right side of Figure 4). This difference in the hard X-ray pulse profiles possibly arises due to the faintness of the source at hard X-rays, combined with the presence of a systematic uncertainty in the LAXPC background measurement beyond ∼30 keV (refer to Antia et al. 2017; Misra et al. 2017 for information on the LAXPC background).

We define the pulse fraction (PF) of the pulsar in the following manner -

$$PF = \frac{F_{max} - F_{min}}{F_{max} + F_{min}}, \tag{1}$$

where F_{max} and F_{min} correspond to maximum and minimum intensities observed in the profile, respectively. During both the observations, the average values of the PF are found to be ≈32%. To evaluate the changes in PF with energy, we investigated the energy resolved profiles and estimated corresponding pulse fraction which are shown in Figure 6. It can be seen that the PF values increase with energy as seen in several other accretion powered X-ray pulsars (Lutovinov & Tsygankov 2009; Jaisawal et al. 2018). The PF of the pulsar 4U 1909+07, estimated from the *NuSTAR* and *Astrosat* observations are comparable up to 30 keV, beyond which the PF values from *Astrosat* observation decreased significantly (Figure 6). This is possibly due to the presence of systematics in the
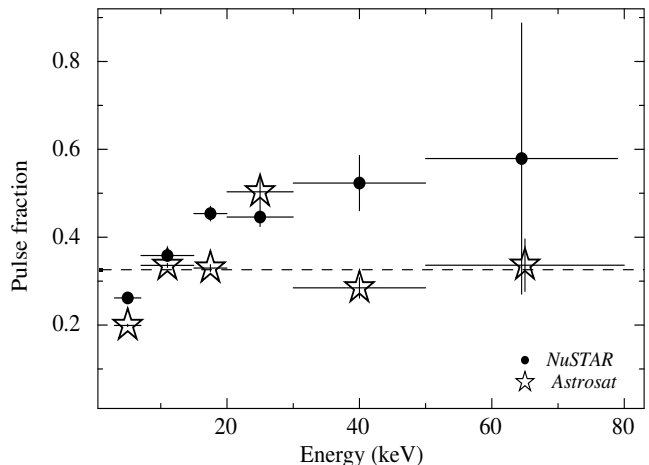
Figure 6. Pulse fraction variation of the pulsar with energy obtained from the light curves in multiple energy bands. The dashed line represents an averaged value of pulse fraction ≈32% estimated from *NuSTAR* and *Astrosat* data in 3-80 keV band.
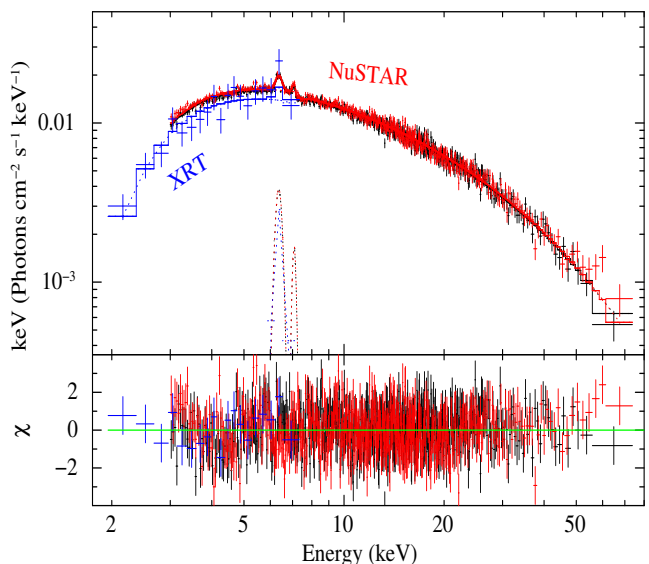

Figure 7. The 1-70 keV energy spectrum of the pulsar obtained from the *Swift*/XRT and *NuSTAR* observations in 2015 July. Best fitted energy spectrum and its corresponding spectral residuals are shown in top and bottom panels, respectively.

LAXPC background measurements at high energies (as mentioned earlier).

3.2 Pulse-phase-averaged spectroscopy

The energy spectrum of 4U 1909+07 is investigated to understand its emission characteristics during the *NuSTAR*, *Swift*, and *Astrosat* observations. Standard empirical models were chosen to fit the broadband spectrum of the pulsar in `XSPEC` package (Arnaud 1996). The 1-79 keV spectrum of the pulsar from *Swift*/XRT and *NuSTAR* is considered in our analysis. We also fitted the 1-35 keV energy continuum by using the data from SXT and LAXPC10 & 20 instruments on-board *Astrosat*. We found that an absorbed high
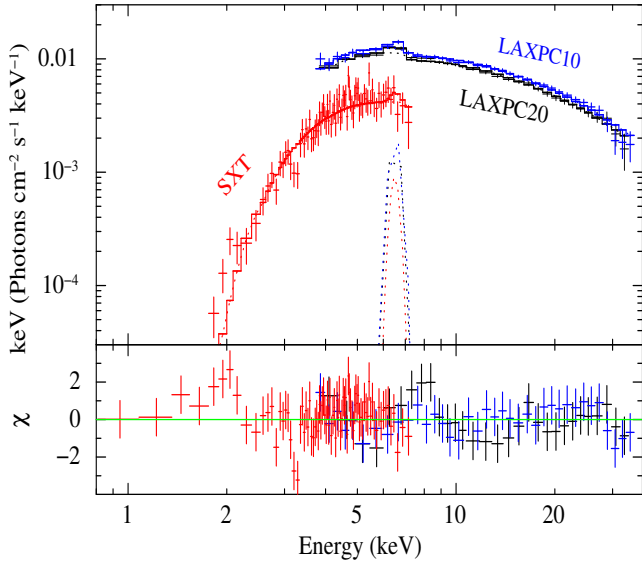
Figure 8. The 1-35 keV energy spectrum of the pulsar obtained from the SXT and LAXPC instruments on-board *Astrosat* in 2017 July. Best fitted energy spectrum and corresponding spectral residuals are shown in top and bottom panels, respectively.

energy cutoff power law model[4] describes these spectra well with the goodness of fit per degree of freedom $\chi_\nu^2 = \chi^2/\nu \approx 1$ in each case (Figures 7 & 8). In the fitting, the contribution for local and interstellar medium absorption N_H observed along the source direction is expressed by TBabs component (Wilms et al. 2000). We also detected iron fluorescence lines at 6.4 and 7.1 keV in the *NuSTAR* spectrum of the source. Any signature of cyclotron absorption line is not found in these observations. Best fitting spectral parameters are given in Table 2. Except for the absorption column density, other components like photon index, folding and cutoff energies are consistent (within the errors) between the 2015 and 2017 data. 4U 1909+07 is found to be strongly obscured owing to a larger column density N_H, in addition to the interstellar absorption of 1.21×10^{22} cm^{-2} along the source direction (HI4PI Collaboration et al. 2016). We estimated the total flux using cflux convolution model in this paper. For a source distance of 4.85 kpc, the 1-80 keV luminosity of the pulsar is measured to be 1.67 and 1.24×10^{36} erg s^{-1} during 2015 and 2017 observations, respectively.

3.3 Pulse-phase-resolved spectroscopy

To investigate the changes in local accreting environment of the pulsar and its effect on the emission geometry, phase-resolved spectroscopy is performed by using the *NuSTAR* data. We extracted pulse-phase resolved spectra in a total of 10 phase bins. Considering appropriate backgrounds, response matrices, and effective areas, the 3-79 keV spectra obtained from FPMA and FPMB detectors are fitted with an absorbed HECut model. In the fitting, we fixed the width of iron lines at the corresponding values obtained from phase-averaged spectroscopy (Table 2). We found that the above model can describe each spectrum well with the value of χ^2/ν close to 1.

---

[4] https://heasarc.gsfc.nasa.gov/xanadu/xspec/manual/Models.html

Table 2. Best-fitting spectral parameters (with 90% errors) of 4U 1909+07 obtained from the *NuSTAR* and *Swift*/XRT observations in 2015 July, and *Astrosat* observation in 2017 July. The fitted model consists of an absorbed high-energy cutoff power law (HECut) with Gaussian components for iron emission lines.

Parameters	*NuSTAR* +*Swift*	*Astrosat*
	HECut	HECut
$N_H{}^a$	10.1±0.5	18±3
Photon index	1.52±0.04	1.5±0.3
E_{cut} (keV)	8.0±0.3	7±3
E_{fold} (keV)	26±1	23±8
Emission lines		
Line energy (keV)	6.36±0.03	6.5
Eq. width (eV)	90±14	154±66
Line energy (keV)	7.1±0.1	–
Eq. width (eV)	27±10	–
Source flux^b		
Flux (1-30 keV)	4.93±0.05	3.7±0.2
Flux (1-80 keV)	5.92±0.06	4.4±0.3
χ_ν^2 (ν)	1.12 (1001)	0.91 (143)

^{a} : Equivalent hydrogen column density in 10^{22} cm^{-2}, ^{b} : Unabsorbed flux in the unit of 10^{-10} erg cm^{-2} s^{-1}.
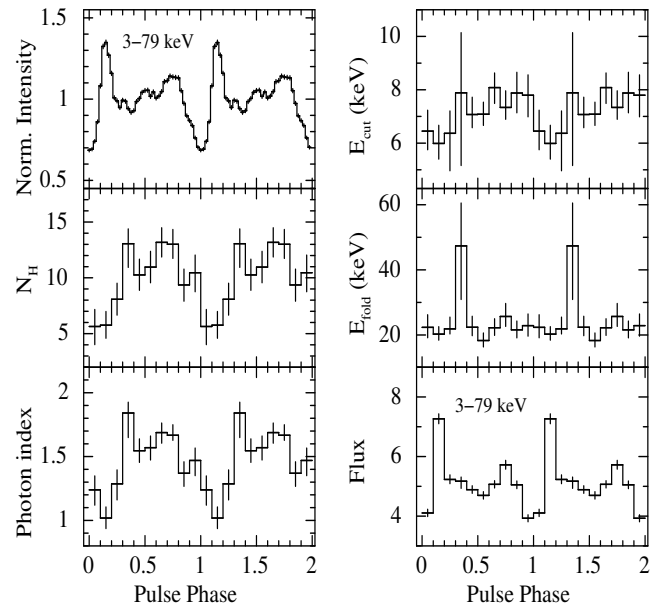

Figure 9. Phase-resolved spectroscopy of 4U 1909+07 using *NuSTAR* data in 2015 July. The first, second, and third panels on left side of the figure show the 3-79 keV pulse profile, absorption column density (10^{22} cm^{-2}), and power-law photon index, respectively. The cutoff energy, folding energy, and the 3-79 keV unabsorbed flux (10^{-10} erg cm^{-2} s^{-1} units) are presented in first, second, and third panels on right side of the figure.

Figure 9 shows the pulse-phase evolution of spectral parameters such as absorption column density, photon index, folding energy, high energy cutoff, and the source flux. The N_H varies between 5 and 15×10^{22} cm^{-2} and is observed to be significantly larger than the expected interstellar absorption (1.21×10^{22} cm^{-2}) along the line of sight. This high value of column density is detected across all pulse-phases of the pulsar, except at 0.1–0.2 phase that coincides with the narrow emission peak in the profile. Corresponding to the changes in the photon index, the spectrum gets softer in the plateau region of the pulse profile. A harder spectrum with a photon index of 1 is detected at 0.1–0.2 pulse-phase of the pulsar. Besides a higher value of the folding energy at a single phase bin (Figure 9), the parameters such as cutoff and folding energies are almost constant (within the error bars) with the pulsar rotation. The change in 3-79 keV source flux with pulse-phase ranges is found to be consistent with the shape of the pulse profile in the same energy range.

4   DISCUSSION AND CONCLUSIONS

We have presented the long term spin period evolution of 4U 1909+07 using the measurements provided by Fürst et al. (2011, 2012), and Jaisawal et al. (2013) along with the recent *NuSTAR* and *Astrosat* observations in this decade. The pulse period of the pulsar has been found to be in globally decline since its discovery (Figure 2). The long term evolution also consists of local fluctuation that is considered as a random walk like behavior (Fürst et al. 2011). In the case of wind accreting sources like Vela X-1 (Deeter et al. 1989), such behaviour signifies the absence of a persistent accretion disk. However in case of 4U 1909+07, the observed net changes in the pulsar period from 604.7 s to 603.6 s during 2001–2017 (Figure 2), the presence of transient accretion disk can not be entirely ruled out.

4.1   Magnetic field strength of the neutron star

The strength of magnetic field of a neutron star (pulsar) can be directly estimated through the detection of cyclotron resonance scattering features in the broadband spectrum. However, there are only about 35 X-ray pulsars in the spectra of which such features are detected (Jaisawal & Naik 2017; Staubert et al. 2019). In the absence of cyclotron features, however, there are alternative methods such as based on the evolution of the spin period or by determining the propeller regime through which the strength of the pulsar magnetic field has been estimated (Ghosh & Lamb 1979; Tsygankov et al. 2016). We can calculate the magnetic field of a pulsar based on the magnetospheric plasma interaction and the spin period evolution. The accreted material carries angular momentum that exerts a torque on the neutron star magnetosphere when the coupling happens at the boundary (Ghosh & Lamb 1979). The neutron star gets spin-up or spin-down depending on the nature of the net torque applied to the magnetosphere. The accretion in the binary system usually takes place through the formation of an accretion disk under Roche-Lobe overflow or through the capture of stellar wind from the companion star. In case of disk accretion, the specific angular momentum of matter ωR_A^2 exceeds the Keplerian specific angular momentum $\sqrt{GMR_A}$ close to Alfvén or magnetospheric radius. For stellar wind accretion, the specific angular momentum of the captured material is considered to be significantly low, thus leading the material to fall straight on the neutron star magnetosphere without any disk-formation (Ho et al. 1989; Frank et al. 2002).
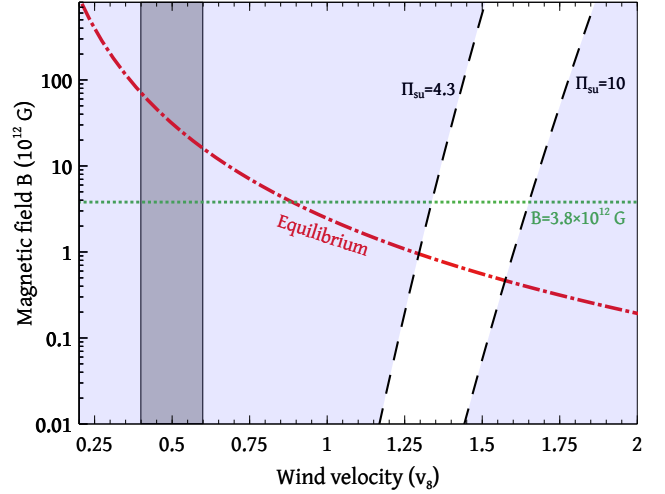
Figure 10. Magnetic field vs. wind velocity relation for 4U 1909+07. The dashed lines (black) indicates the variation between magnetic field and wind velocity (in a unit of 10^8 cm s^{-1}) for a given parameter Π_{su} of the settling accretion theory at 4.3 and 10 (white region). The dash-dot red curve shows the magnetic field in case of spin equilibrium. Observed wind velocity of the optical companion is also shown in the grey range. The dashed horizontal line (green) corresponds to the magnetic field estimated by a tentative estimation of cyclotron line (Jaisawal et al. 2013)

.

Two types of quasi-spherical wind accretion onto the neutron stars are expected (Shakura et al. 2012, 2018). The supersonic quasi-spherical accretion, also known as the Bondi-Hoyle-Littleton accretion, occurs when the accreting shocked plasma rapidly cools down and falls supersonically towards the magnetosphere. The subsonic quasi-spherical accretion is possible in slow rotating magnetized neutron star with X-ray luminosity $<4 \times 10^{36}$ erg s^{-1} where the accreted plasma remains hot at the magnetospheric boundary, (Shakura et al. 2012). In the latter case, the material forms a hot quasi-static shell around the rotating neutron star magnetosphere in process of setting subsonically. This shell mediates the angular momentum transfer to- or from the neutron star by large-scale convective turbulent structures. The spin-up or spin-down of the neutron stars are expected to observe depending on the sign of angular velocity difference between the magnetosphere and the accreting material. The model can successfully explain the secular spin variation of the pulsar along with any irregular short-term frequency fluctuations.

We apply the quasi-spherical settling accretion theory estimating the magnetic field of 4U 1909+07 from the applied torque. According to the theory (Shakura et al. 2012; Equation 4 of Postnov et al. 2015), the spin-up rate is

$$\dot{\omega}_{su} \simeq 10^{-9} [Hz\ d^{-1}]\ \Pi_{su}\ \mu_{30}^{1/11}\ v_8^{-4} \left(\frac{P_b}{10\ d} \right)^{-1} \dot{M}_{16}^{7/11} \quad (2)$$

here the spin rate $\dot{\omega}_{su}$ is measured to be 2.56×10^{-9} [Hz d^{-1}] for 4U 1909+07. Π_{su} is a system independent dimensionless parameter of the theory ranging between 4.3 and 10 (Shakura et al. 2012; Postnov et al. 2015; Shakura et al. 2018). The dipole magnetic moment of the neutron star is $\mu_{30} = \mu/10^{30}$[G cm^3] and is related to the magnetic field (B) by expression $\mu = BR^3/2$ (the neutron star radius R is assumed to be 10 km). The parameter v_8 is the stellar wind velocity in the unit of 10^8[cm s^{-1}]. The mass accretion rate $\dot{M}_{16} = \dot{M}/10^{16}$[g s^{-1}] is estimated to be $\dot{M}_{16} = 0.69$ for the source

luminosity of 1.24×10^{36} erg s^{-1} at 20% accretion efficiency. The orbital period P$_b$ of the system is 4.4 d. In this regime, the magnetic field strongly depends on the wind velocity that has been estimated to be 500 ± 100 km s^{-1} for 4U 1909+07 (Martínez-Núñez et al. 2015). We found that the settling model requires approximately three times higher wind velocity for 4U 1909+07 between 1300–1500 km s^{-1} to get a magnetic field in a range of 10^{12}–10^{14} G (white region in Figure 10) for a given value of Π_{su}. We can not adequately determine the magnetic field using Equation 2 of the settling accretion theory.

We notice that the observed source luminosity is stable at $\sim 10^{36}$ erg s^{-1} during each X-ray observations so far. Despite the variation in spin period, considering an extreme case, we may assume the pulsar is accreting close to its equilibrium spin period that is :

$$P_{eq} \simeq 940[s] \, \mu_{30}^{12/11} v_8^4 \left(\frac{P_b}{10 \, d} \right) \dot{M}_{16}^{-4/11} \qquad (3)$$

The above equation is adopted from Shakura et al. (2012) & Postnov et al. (2015). Considering the wind velocity between 400–600 km s^{-1} and the observed mass accretion rate, the spin equilibrium magnetic field can be estimated to be $>10^{13}$ G (red curve in Figure 10). The inferred value is within a factor of five times higher than the polar magnetic field ($\approx 7.6 \times 10^{12}$ G – twice the equatorial field) inferred from the tentative detection of cyclotron line by Jaisawal et al. (2013) which has not yet been re-confirmed. The measurement appears to be reasonable, given many theoretical uncertainties, as well as the fact that the pulsar is not strictly at equilibrium due to changes in the spin frequency.

4.2 Pulse profile and spectroscopy

We examine the emission geometry of the pulsar using the *NuSTAR* and *Astrosat* observations in 2015 July and 2017 July, respectively. This is done by studying the pulse profiles that strongly depend on the energy. We observed a complex, broad profile in soft X-rays that evolves into a narrow emission peak followed by plateau like structure in hard X-rays. Almost similar energy evolution and pulse morphology were detected in the earlier studies (Fürst et al. 2011, 2012; Jaisawal et al. 2013). The existence of anomalous pulse profiles at several epochs advocates the persistent emission geometry of the pulsar. Even so, the marginal difference in the profile morphology exists that possibly led by the local variation in column density and distribution of the stellar wind across the binary orbit.

The emission from one or both the poles of the neutron star produces a relatively complex pulse profile depending on the geometrical and gravitation effects (Kraus et al. 1995; Bulik et al. 2003; Lutovinov & Tsygankov 2009; Sasaki et al. 2012). The absorption of soft X-ray photons emitted from the accretion column by the accreting material complicates the profile further. Sometimes this material influences the direct pulsar emission so much that multiple absorption dips are observed at definite pulse phases of the pulsar. Such dips have been frequently seen in the pulse profiles of Be/X-ray binary pulsars during X-ray outbursts (see e.g., Maitra et al. 2012; Naik et al. 2013; Jaisawal et al. 2016; Ferrigno et al. 2016; Epili et al. 2017; Gupta et al. 2018). In the present study, the accretion columns at both the poles of the pulsar contribute as the pulse profiles below 10 keV are seen to be double-peaked. We observed a narrow emission peak in a 0.1–0.2 phase range of the pulse profile at higher energies. The detection of high pulse fraction (about 50%) above 20 keV is expected from a narrow emission region (Figure 3).

The energy spectrum of pulsars originates from thermal and bulk Comptonization physical processes in the accretion column (Becker & Wolff 2007). The emission from 4U 1909+07 can be described by an absorbed HECut model as seen during the 2015 and 2017 observations. The spectral parameters are consistent during these observations, except the value of the column density. N_H is detected to be high 18×10^{22} cm^{-2} during the *Astrosat* observation, covering 0.87–0.05 orbital phase range. We also observed a relatively lower value of column density 10×10^{22} cm^{-2} using *NuSTAR* and XRT data obtained in 0.215–0.437 orbital phase range. These variations are in agreement with the findings by Levine et al. (2004). The authors also found a strong increase in N_H below 0.12 orbital phase. The orbital changes in the column density can be explained by considering the movement of the neutron star through the inhomogeneously distributed stellar wind. To probe the wind distribution further, we performed phase-resolved spectroscopy using *NuSTAR* data in 2015. We detected a phase variation in the N_H which likely affects the X-ray emission from the accretion column. The N_H is found to be three times higher in the plateau region of the pulse profile as opposed to the value observed at 0.1–0.2 pulse phase. A narrow emission peak is clearly present 0.1–0.2 pulse phase range when the column density is low.

The cyclotron absorption line is understood to originate from the resonant scattering of photons with the electrons in the quantized Landau levels (Meszaros 1992). These features are observed in the 10–100 keV energy range of pulsar spectrum corresponding to a magnetic field of 10^{12}–10^{13} Gauss, based on the 12-B-12 rule (Jaisawal & Naik 2017; Staubert et al. 2019). A cyclotron line was tentatively observed at 44 keV in 4U 1909+07 using the *Suzaku* data (Jaisawal et al. 2013). However, in the present study, any signature of a cyclotron absorption line in phase-averaged and phase-resolved spectroscopy of the pulsar spectrum is not detected. The spin-equilibrium magnetic field can match the polar B-strength provided by cyclotron line within a factor of 5, possibly due to the theoretical uncertainties in the calculation. Future longer exposure observations with instruments like *NuSTAR*, *Astrosat*, and the proposed *STROBE-X* mission (Ray et al. 2019a) could confirm the detection/ non-detection of a cyclotron absorption feature in 4U 1909+07.

DATA AVAILABILITY

We used archival data of *NuSTAR*, *Swift*, and *Astrosat* observatories for this work.

REFERENCES

Agrawal P. C., 2006, Advances in Space Research, 38, 2989
Agrawal P. C., et al., 2017, Journal of Astrophysics and Astronomy, 38, 30
Antia H. M., et al., 2017, ApJS, 231, 10
Arnaud K. A., 1996, in Jacoby G. H., Barnes J., eds, Astronomical Society of the Pacific Conference Series Vol. 101, Astronomical Data Analysis Software and Systems V. p. 17
Basko M. M., Sunyaev R. A., 1975, Astronomy and Astrophysics, 42, 311
Becker P. A., Wolff M. T., 2007, ApJ, 654, 435
Bulik T., Gondek-Rosińska D., Santangelo A., Mihara T., Finger M., Cemeljic M., 2003, A&A, 404, 1023
Caballero I., Wilms J., 2012, Memorie della Societa Astronomica Italiana, 83, 230
Corbet R. H. D., Krimm H. A., 2013, ApJ, 778, 45
Deeter J. E., Boynton P. E., Lamb F. K., Zylstra G., 1989, ApJ, 336, 376
Epili P., Naik S., Jaisawal G. K., Gupta S., 2017, MNRAS, 472, 3455
Evans P. A., et al., 2009, MNRAS, 397, 1177
Farinelli R., Ceccobello C., Romano P., Titarchuk L., 2012, A&A, 538, A67
Ferrigno C., Pjanka P., Bozzo E., Klochkov D., Ducci L., Zdziarski A. A., 2016, A&A, 593, A105
Forman W., Jones C., Cominsky L., Julien P., Murray S., Peters G., Tananbaum H., Giacconi R., 1978, The Astrophysical Journal Supplement Series, 38, 357
Frank J., King A., Raine D. J., 2002, Accretion Power in Astrophysics: Third Edition
Fürst F., Kreykenbohm I., Suchy S., Barragán L., Wilms J., Rothschild R. E., Pottschmidt K., 2011, A&A, 525, A73
Fürst F., Pottschmidt K., Kreykenbohm I., Müller S., Kühnel M., Wilms J., Rothschild R. E., 2012, A&A, 547, A2
Ghosh P., Lamb F. K., 1979, ApJ, 234, 296
Giacconi R., Murray S., Gursky H., Kellogg E., Schreier E., Matilsky T., Koch D., Tananbaum H., 1974, The Astrophysical Journal Supplement Series, 27, 37
Gupta S., Naik S., Jaisawal G. K., Epili P. R., 2018, MNRAS, 479, 5612
HI4PI Collaboration et al., 2016, A&A, 594, A116
Harrison F. A., et al., 2013, ApJ, 770, 103
Ho C., Taam R. E., Fryxell B. A., Matsuda T., Koide H., 1989, MNRAS, 238, 1447
Jaisawal G. K., Naik S., 2017, in Serino M., Shidatsu M., Iwakiri W., Mihara T., eds, 7 years of MAXI: monitoring X-ray Transients, held 5-7 December 2016 at RIKEN. p. 153 (arXiv:1705.05536)
Jaisawal G. K., Naik S., Paul B., 2013, ApJ, 779, 54
Jaisawal G. K., Naik S., Epili P., 2016, MNRAS, 457, 2749
Jaisawal G. K., Naik S., Chenevez J., 2018, MNRAS, 474, 4432
Jaisawal G. K., et al., 2019, ApJ, 885, 18
Kraus U., Nollert H. P., Ruder H., Riffert H., 1995, ApJ, 450, 763
Leahy D. A., 1987, A&A, 180, 275
Levine A. M., Rappaport S., Remillard R., Savcheva A., 2004, The Astrophysical Journal, 617, 1284
Lewin W. H. G., van Paradijs J., van den Heuvel E. P. J., 1997, X-ray Binaries
Lutovinov A. A., Tsygankov S. S., 2009, Astronomy Letters, 35, 433
Maitra C., Paul B., Naik S., 2012, MNRAS, 420, 2307
Martínez-Núñez S., Sander A., Gímenez-García A., Gónzalez-Galán A., Torrejón J. M., Gónzalez-Fernández C., Hamann W. R., 2015, A&A, 578, A107
Martínez-Núñez S., et al., 2017, Space Sci. Rev., 212, 59
Meszaros P., 1992, High-energy radiation from magnetized neutron stars
Misra R., et al., 2017, ApJ, 835, 195
Morel T., Grosdidier Y., 2005, MNRAS, 356, 665
Nagase F., 1989, PASJ, 41, 1

Naik S., Paul B., Ali Z., 2011, ApJ, 737, 79
Naik S., Maitra C., Jaisawal G. K., Paul B., 2013, ApJ, 764, 158
Odaka H., Khangulyan D., Tanaka Y. T., Watanabe S., Takahashi T., Makishima K., 2013, ApJ, 767, 70
Paul B., Naik S., 2011, Bulletin of the Astronomical Society of India, 39, 429
Porter J. M., Rivinius T., 2003, PASP, 115, 1153
Postnov K. A., Mironov A. I., Lutovinov A. A., Shakura N. I., Kochetkova A. Y., Tsygankov S. S., 2015, MNRAS, 446, 1013
Ramadevi M. C., et al., 2018, Journal of Astrophysics and Astronomy, 39, 11
Rao A. R., Bhattacharya D., Bhalerao V. B., Vadawale S. V., Sreekumar S., 2017, Current Science, 113, 595
Ray P. S., et al., 2011, ApJS, 194, 17
Ray P. S., et al., 2019a, arXiv e-prints, p. arXiv:1903.03035
Ray P. S., et al., 2019b, ApJ, 879, 130
Reig P., 2011, Ap&SS, 332, 1
Reig P., Nespoli E., 2013, A&A, 551, A1
Revnivtsev M., Mereghetti S., 2015, Space Sci. Rev., 191, 293
Sasaki M., Müller D., Kraus U., Ferrigno C., Santangelo A., 2012, A&A, 540, A35
Shakura N., Postnov K., Kochetkova A., Hjalmarsdotter L., 2012, MNRAS, 420, 216
Shakura N., Postnov K., Kochetkova A. r., Hjalmarsdotter L., 2018, Quasi-Spherical Subsonic Accretion onto Magnetized Neutron Stars. p. 331, doi:10.1007/978-3-319-93009-1_7
Singh K. P., et al., 2017, Journal of Astrophysics and Astronomy, 38, 29
Staubert R., et al., 2019, A&A, 622, A61
Tandon S. N., et al., 2017, AJ, 154, 128
Tauris T. M., van den Heuvel E. P. J., 2006, Formation and evolution of compact stellar X-ray sources. pp 623–665
Torrejón J. M., Schulz N. S., Nowak M. A., Kallman T. R., 2010, ApJ, 715, 947
Tsygankov S. S., Lutovinov A. A., Doroshenko V., Mushtukov A. A., Suleimanov V., Poutanen J., 2016, A&A, 593, A16
Vasilopoulos G., Petropoulou M., Koliopanos F., Ray P. S., Bailyn C. B., Haberl F., Gendreau K., 2019, MNRAS, 488, 5225
Vasilopoulos G., et al., 2020, MNRAS, 494, 5350
Walter R., Lutovinov A. A., Bozzo E., Tsygankov S. S., 2015, Astronomy and Astrophysics Review, 23, 2
Wen L., Remillard R. A., Bradt H. V., 2000, The Astrophysical Journal, 532, 1119
White N. E., Swank J. H., Holt S. S., 1983, ApJ, 270, 711
Wilms J., Allen A., McCray R., 2000, ApJ, 542, 914
Wilson-Hodge C. A., et al., 2018, ApJ, 863, 9

This paper has been typeset from a T_EX/L^AT_EX file prepared by the author.